Advances in Science and Technology Research Journal

Advances in Science and Technology Research Journal, 2026, 20(6), 262–272
https://doi.org/10.12913/22998624/217660
ISSN 2299-8624, License CC-BY 4.0

Received: 2026.01.05
Accepted: 2026.04.15
Published: 2026.05.01

Assessment of friction conditions on the edge of sheet metal forming tools under dry friction conditions

Tomasz Trzepieciński[1], Krzysztof Szwajka[2*], Joanna Zielińska-Szwajka[2], Marek Szewczyk[2]

[1] Faculty of Mechanical Engineering and Aeronautics, Rzeszów University of Technology, Al. Powst. Warszawy 8, 35-029 Rzeszów, Poland
[2] Faculty of Mechanics and Technology, Rzeszów University of Technology, ul. Kwiatkowskiego 4, 37-450 Stalowa Wola, Poland
* Corresponding author's e-mail: kszwajka@prz.edu.pl

ABSTRACT

This article presents the results of studies on friction conditions at the rounded edge of stamping dies in sheet metal forming. Using a friction tester developed by the authors to perform a bending-under-tension test, low-carbon steel sheets were examined under dry friction conditions. Changes in friction conditions were achieved by producing functional surfaces on the countersample surfaces using electron beam melting and ion implantation. The coefficient of friction was determined using two strategies: with a stationary countersample and with a freely rotating countersample. The influence of the surface treatment of the countersamples on friction-induced changes in the surface roughness of the sheet metal was also evaluated. The difference in the friction coefficient between the two analyzed friction test strategies ranged from 1.78% to 8.51%, depending on the type of friction pair. Similarly, the friction process led to an increase in the mean surface roughness Sa (by 1.34–16.7%) and the skewness Ssk (by 9.7–70.9%). Depending on the friction pair type and the method of countersample mounting, the strain-induced kurtosis Sku of the strip samples decreased by 10.2–42.4%.

Keywords: friction mechanism, low-carbon steel sheet, metal forming, tribology.

INTRODUCTION

Sheet metal forming is one of the basic methods of producing finished products in the automotive industry, the household appliance industry, and construction. Sheet metal forming operations are associated with a number of technological problems, such as strain-induced reduction in the ductility of the workpiece material [1], the springback phenomenon [2], dimensional and shape inaccuracies of products [3], and deterioration of component surface quality [4]. One of the phenomena that must be taken into account when designing a forming process is friction, which depends on many factors related to the surface topography of the sheet metal [5] and the tools [6], surface processing methods [7], lubrication conditions [8], forming temperature [9], and contact pressures [10]. Accurate identification of friction conditions in a given technological process is hindered by strain-induced: (i) continuous evolution of the sheet surface topography [11] and (ii) changes in the mechanical properties of the sheet due to the work-hardening phenomenon [12].

The largest deformations occur at the edges of the punch and die, where the sheet is subjected to bending, most often at an angle of 90°. Bending under tension (BUT) friction tests [13] are used to identify frictional resistance in this region. While studies using the strip drawing test are generally widespread, friction tests addressing conditions at tool edges are very limited. One explanation for this situation is the lack of commercially available tribotesters for conducting BUT friction tests, which necessitates the

development and fabrication of such tribotesters by researchers themselves [6,14]. Chronologically, the first reports on BUT tests appeared in the works of Duncan et al. [15] and Fox et al. [16]. Researchers have investigated the influence of lubrication conditions [15], lubricant type [17], sliding speed [17], wrap angle [16], sheet orientation, specimen material [14, 16], countersample radius [14], and mechanical properties of sheets (the ratio of tensile strength to yield strength) [15] on the value of the coefficient of friction (CoF). Duncan et al. [15] reported that sheet orientation and corner radius have only a very minor effect on the CoF. Fox et al. [16] found that, with increasing wrap angle, the ratio between forward-tension force and back-tension force changes, causing the CoF to vary nonlinearly with increasing front-tension force. Han [14], investigating different sheet grades, concluded that the CoF increases with increasing tool curvature. A significant decrease in the CoF with increasing sliding speed was observed by Andreasen et al. [17] for all analysed lubrication conditions.

The results of studies available in the literature on friction at punch edges mainly concern friction under lubricated conditions. Meanwhile, at the punch edge in sheet metal forming, dry friction is more advantageous than lubricated conditions because dry friction reduces the total forming force and increases the formability of the sheet, as reported by Gierzyńska [18]. Surface treatment by electron beam melting and ion implantation is considered a means of engineering surfaces that allow an increase in the CoF under dry friction conditions without a significant increase in sheet surface roughness compared to the uncoated base material. Based on the identified gap in the literature, the aim of this article is to investigate the friction of low-carbon steel DC01 sheets under dry friction conditions using countersamples with different surface topographies. In addition, to better identify the influence of process parameters on friction, the CoF was determined using different process strategies. Friction-induced and strain-induced changes in sheet surface roughness were also evaluated. The friction tests presented in this study can be related to industrial forming of DC01 sheet metal under dry friction conditions at the punch edge, with a sliding speed of 30 mm/min and using a punch with an edge radius of 15 mm.

MATERIALS AND METHODS

Test material

When selecting the test material, the authors intended to use a steel sheet metal grade commonly applied in the deep drawing operations. Therefore, a low-carbon DC01 steel sheet with a thickness of 0.8 mm was used. This sheet contains no more than 0.12 wt.% carbon, which ensures good formability in sheet forming operations. Uniaxial tensile tests conducted in accordance with the ISO 6892-1 standard made it possible to determine the yield strength (163 MPa), tensile strength (290 MPa), and elongation A_{50} (38%). Due to the character of the investigations presented in this article, which focus on friction, the surface topography of the sheet was measured using a T8000RC measuring station. The surface topography together with the main roughness parameters and the distribution of the height ordinate are presented in Figure 1a and 1b, respectively. The roughness parameters and the bearing area curve parameters were determined in accordance with ISO 25178 and ISO 4287 standards, respectively.

Friction tester

A self-fabricated tribotester simulating friction conditions at the rounded edges of a stamping tool was used in the experiments. The test consists of stretching a strip sample around a roller (cylindrical countersample - CS) with a radius of 15 mm and a wrap angle of 90°. One end of the sample is fixed, while a load is applied to the other end (Figure 2). During the test, the applied forward-tension (F_{FT}) force and the back-tension (F_{BT}) force are measured. In general, two variants of the test are distinguished. In the first variant, the sample is stretched around a fixed cylindrical CS. In the second variant, the test is carried out in two stages. In the first stage, the sample is stretched around a stationary CS (Figure 2a), and in the second stage, it is stretched around a freely rotating CS (Figure 2b). Values of stretching forces from both stages are required to determine the CoF. The stretching speed of the strip sample around the counter-sample was 30 mm/min. The test continued until the sheet metal strip broke. The tests were conducted under controlled displacement conditions. The test temperature was 24.5 °C.

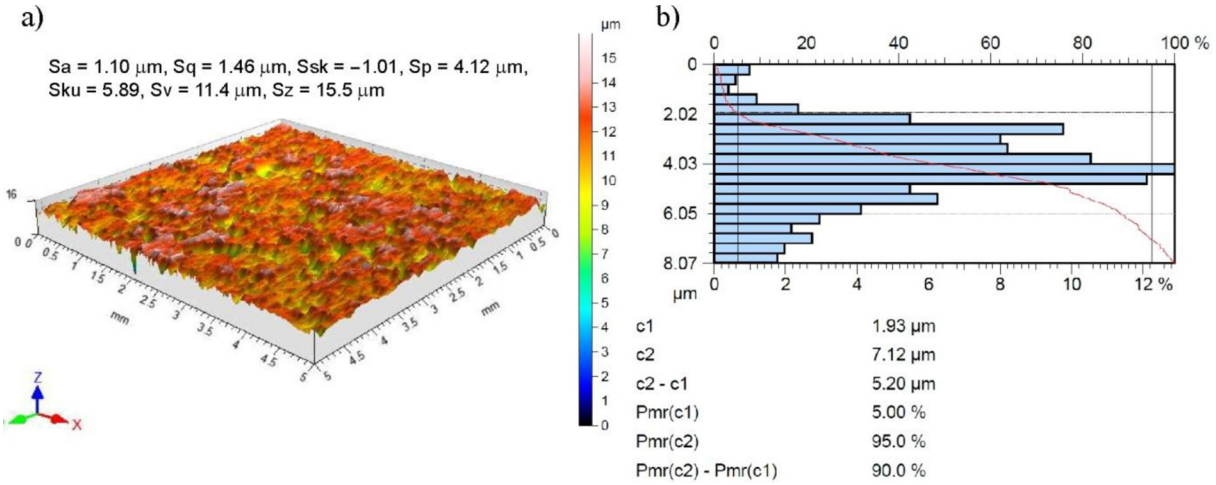

Figure 1. a) surface topography and b) the material ratio curve of surface of the test material

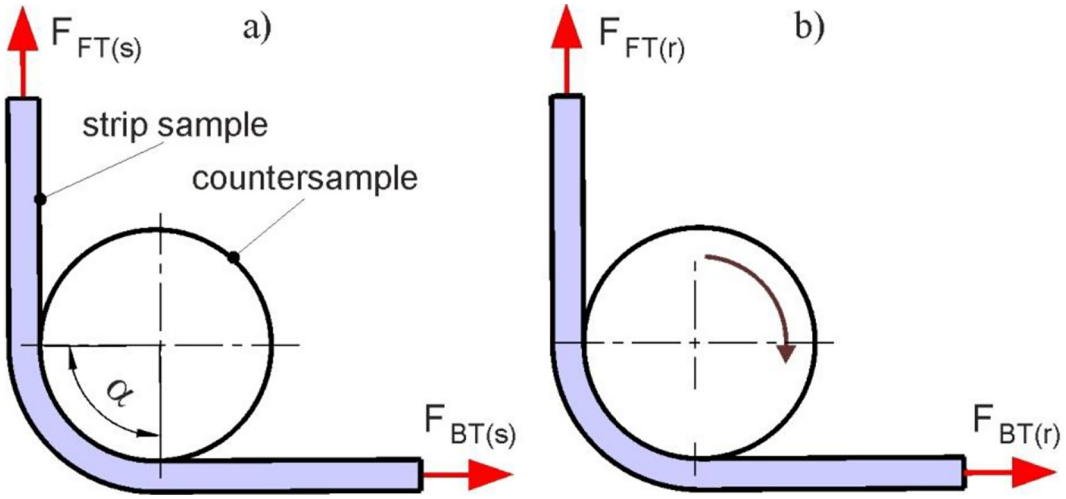

Figure 2. Schematic of friction test under a) a stationary and b) freely rotating CS

Photograph of the tribotester and a schematic of the force measurement channels are shown in Figure 3. The tester was mounted in the lower grip of a Zwick Z100 universal testing machine. The upper grip held one end of a strip sample with a width of 18 mm and a length of 400 mm. Construction details of the device can be found in a previous study [19].

Changes in friction conditions can be achieved by modifying the surface topography of the CSs and their tribological properties. The aim of the study was to determine the effect of electron beam melting (EBM) and ion implantation (IO) of Pb on friction conditions in the considered friction test. A cylinder made of cold-work tool steel 145Cr6 was used as the reference CS. Detailed procedures of the EBM and IO processes were described in a previous study [6].

The surfaces after treatment were characterized by different topographies and surface roughness values (Figure 4). Three of the considered CSs (145Cr6, 145Cr6+IO, and 145Cr6+EBM+IO) exhibited similar values of average roughness and kurtosis. The average roughness of the EBM-processed CS was more than half that of the remaining CSs (Figure 4). The tests were conducted under dry friction conditions. Prior to the friction process, the surfaces of both the samples and the CSs were cleaned with acethone. The samples were washed in a container with acetone and then left to dry for 48 hours in a dry environment at ambient temperature.

This article compares two strategies for determining the CoF using a sheet metal stretching test around a cylindrical CS. In the first strategy, the test involves testing friction using a stationary CS (Figure 2a). According to Duncan et al.

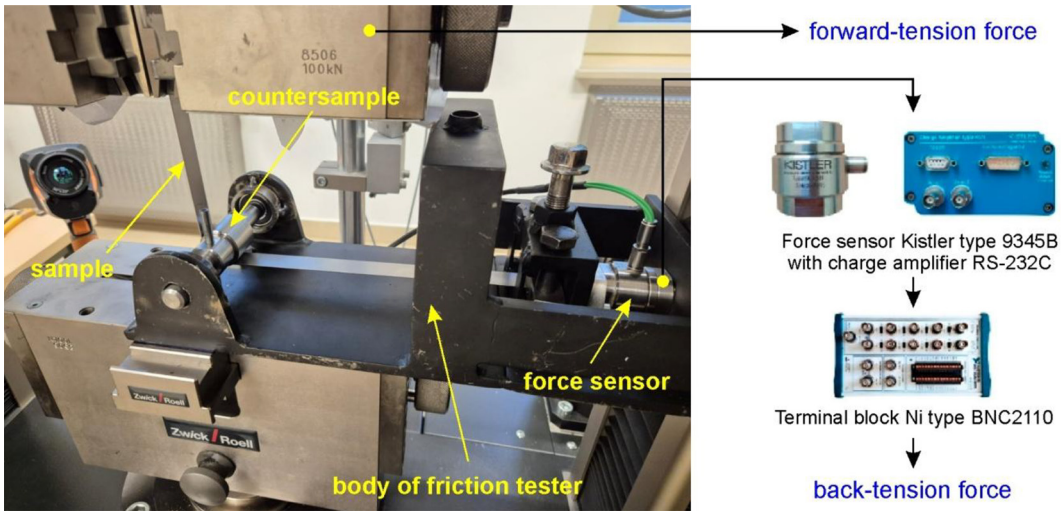

Figure 3. Schematic diagram of the tribotester and force measurement channels

[15] summation of forces F in tangential direction (along the contact surface) gives:

$$\frac{dF}{F} = \mu \cdot d\alpha \tag{1}$$

Assuming a constant value of CoF [15], integration of Equation 1 gives:

$$\frac{F_1}{F_2} = e^{\left(\frac{\mu\pi}{2}\right)} \tag{2}$$

After transforming Equation 2 and substituting $F_{FT(s)}$ for F_1 (Figure 2a) and $F_{BT(s)}$ for F_2 (Figure 2a), we get:

$$\mu = \frac{2}{\pi} ln \frac{F_{FT(s)}}{F_{BT(s)}} \tag{3}$$

In the second considered strategy for determining the CoF, the test is carried out in two stages; featuring a stationary CS and freely rotating CS. To determine the CoF, Fox et al. [16] modified Equation 3 by taking into account the bending force of the sheet metal around the CS (Swift bending tension) F_B:

$$\mu = \frac{2}{\pi} ln \frac{F_{FT(s)} - F_B}{F_{BT(s)}} \tag{4}$$

where: F_B is the difference between the forward-tension force $F_{FT(r)}$ and back-tension force $F_{BT(r)}$ determined using freely rotating CS (Figure 2b). Then Equation 4 can be written as:

$$\mu = \frac{2}{\pi} ln \frac{F_{FT(s)} - \left(F_{FT(r)} - F_{BT(r)}\right)}{F_{BT(s)}} \tag{5}$$

RESULTS AND DISCUSSION

BUT test forces

The experiments were conducted using a stationary CS and a freely rotating CS. As a result, for each combination of the friction pair, a set of data consisting of forward-tension and back-tension forces was obtained (Figure 5). The elongation of the samples during the test was measured according to the following equation:

$$\varepsilon = \frac{l_k}{l_0} \cdot 100\% \tag{6}$$

where: l_k is the actual elongation of the sample, and l_0 is the initial length of the sample between the grips.

Friction is a phenomenon that significantly limits the elongation of samples during the BUT test. For all friction pairs, the elongation corresponding to the onset of necking was approximately twice as small under friction conditions involving a stationary roller compared to the test with a freely rotating roller. In addition, under friction conditions with a stationary roller, signs of the stick–slip phenomenon were observed, manifested by local fluctuations in the process forces (Figure 5). The friction phenomenon does not affect the tensile behavior of the sample material; therefore, the maximum front-tension forces are the same for both test configurations and amounts to approximately 4.000 N (Figure 5). Under friction conditions with a stationary roller, a clear difference between the $F_{FT(s)}$ and $F_{BT(s)}$ forces is

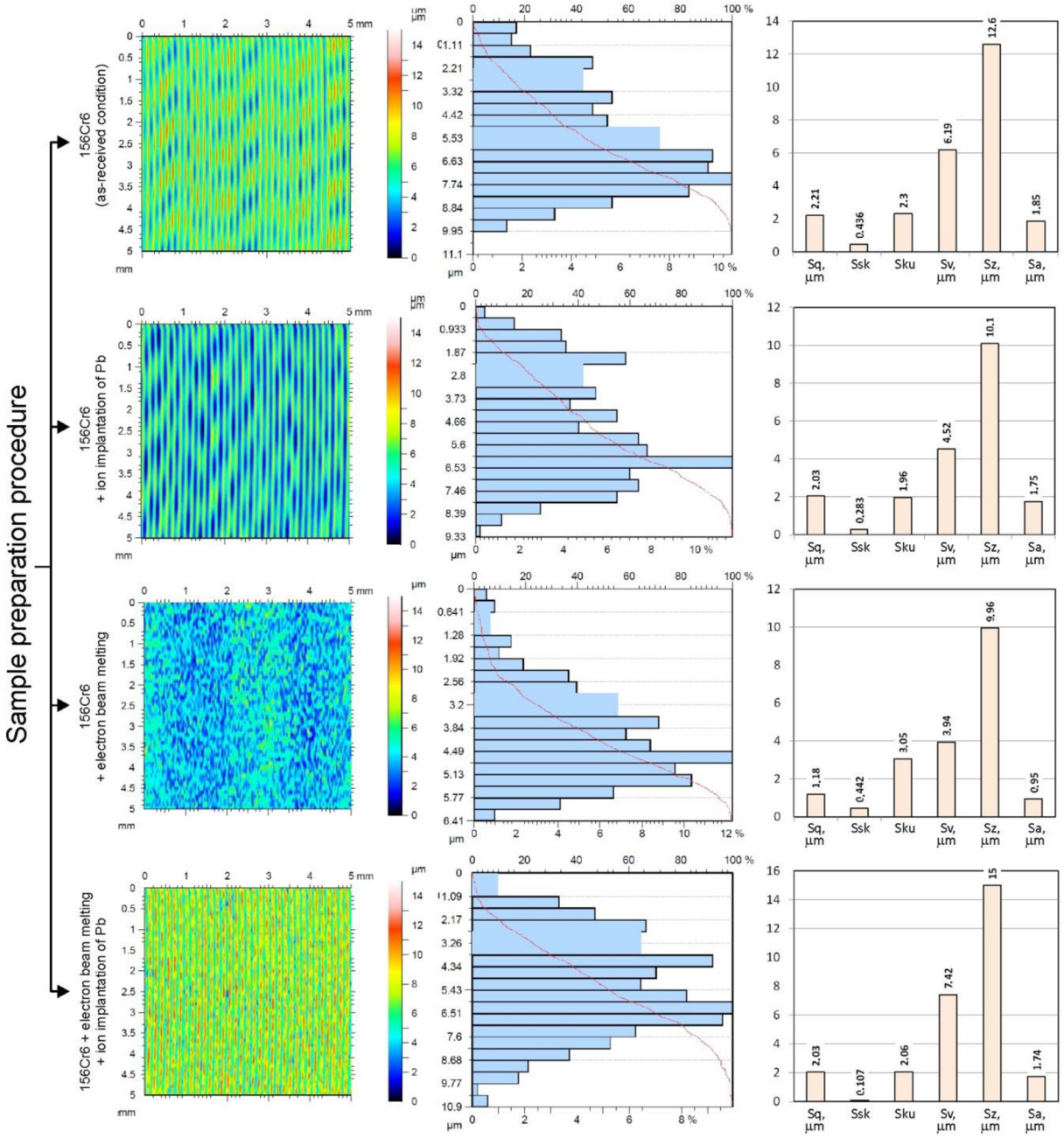

Figure 4. Topography, bearing area curves and basic surface roughness parameters of the CSs

observed, resulting from frictional resistance between surfaces of the strip sample and the roller.

Coefficient of friction

A comparison of the CoFs determined using Equations 3 and 5 for all friction pairs is presented in Figure 6. The initial unstable variation of the friction coefficient is associated with the running-in stage, during which the load-bearing surface of the specimen is formed as a result of asperity flattening. This stage ends after approximately 3–4% elongation of the sample, depending on the type of friction pair (Figure 6). After the running-in stage, the CoF stabilizes until the onset of necking and the subsequent failure of the specimen. A clear influence of the friction pair type on the CoFs determined using the two considered equations can be observed. For the 145Cr6/DC01 (Figure 6a) and 145Cr6+IO/DC01 (Figure 6d) friction pairs, higher friction coefficients were obtained using Equation 5. In contrast, for the remaining friction pairs (Figures 6b and 6c), Equation 3 yielded higher friction coefficients. This difference results from the inclusion of the Swift bending tension F_B in Equation 5 and from

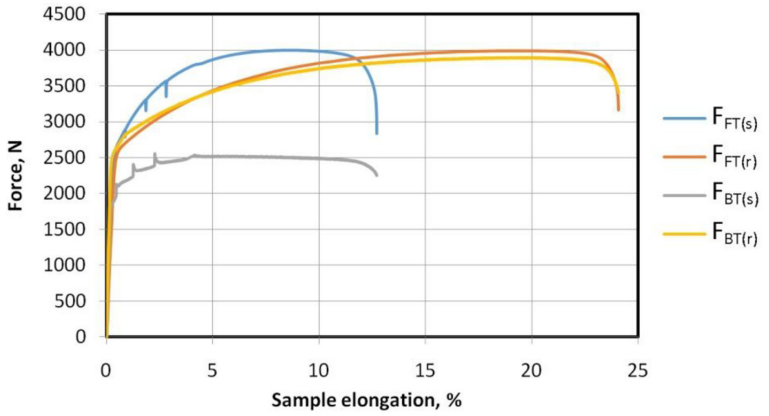

Figure 5. Changes in process forces during BUT test involving stationary and freely rotating EBM CS

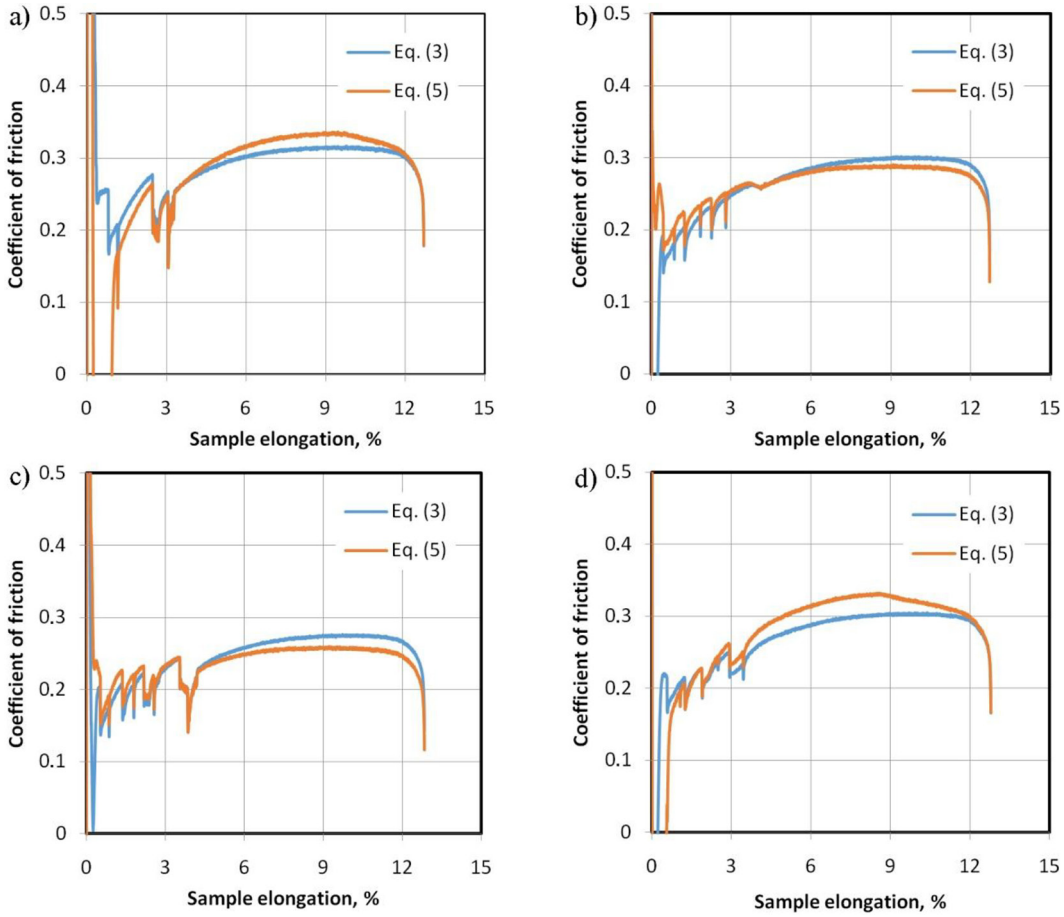

Figure 6. Influence of sample deformation on the change of CoF during friction with the following CSs: a) 145Cr6, b) 145Cr6+EBM, c) 145Cr6+IO and d) 145Cr6+EBM+IO

the influence of different friction-pair surface topographies on the character of specimen sliding around the roller. As a result of the friction process in the BUT test at a 90° bending angle, the strip sample bends away from the tensile direction, as demonstrated in previous studies [20]. This disturbance affects the value of the F_B force and, consequently, the CoF.

To more precisely identify the effect of the type of friction pair on the CoF, the difference (D) between the CoFs determined from Equations 3 and 5 was calculated for various instantaneous values of sheet deformations ε ranging from 6 to 12% (Table 1). The coefficient of friction values for each sample and countersample configuration were determined based on two repetitions.

Standard deviation values are given in parentheses. In the case of the friction pairs 145Cr6+EBM/DC01 and 145Cr6+IO/DC01, the Equation 5 that accounts for the Swift bending tension F_B yielded higher values of the CoF than Equation 3. In addition, for these friction pairs, an increase in sheet deformation resulted in an increase in the difference D between the CoF determined from Equations 3 and 5, from approximately 2.09% (ε = 6%) to -7.5% (ε = 8%). For the friction pairs 145Cr6/DC01 and 145Cr6+EBM+IO/DC01, the opposite trend was observed. Higher CoF were obtained using Equation 5, and increasing specimen elongation led to a tendency for the difference D to decrease, from 8.38% to 2.06% in the deformation range ε between 6% and 12% (145Cr6+EBM+IO/DC01).

Surface roughness

Figure 7 shows the effect of the type of CS on friction-induced changes in selected surface roughness parameters of the strip samples. The friction phenomenon caused an increase in the mean surface roughness of the sheet (Figure 7a). However, under stationary roller conditions, the increase in mean roughness was greater. For the friction pair 145Cr6+IO/DC01, the difference in mean roughness values for the two types of roller mounting is the smallest. Although frictional contact leads to the flattening of surface asperity summits, large sheet deformations cause deformation of material grains and their reorientation in accordance with the stretching direction. This results in the formation of a directional topography, which alters the profile height and consequently the mean roughness Sa. As a result of the friction process, the maximum profile height Sz increased only for the friction pairs 145Cr6/DC01 and 145Cr6+IO/DC01 (Figure 7b). For the 145Cr6+EBM/DC01 friction pair, the Sz parameter decreased by 20.6% and 22.6% during tests conducted under stationary CS and freely rotating CS conditions, respectively. However, for the 145Cr6+EBM+IO/DC01 friction pair, the Sz parameter decreased by 10.9% and 19.3% during tests conducted under stationary CS and freely rotating CS conditions, respectively. This may be related to the surface topography of the countersamples produced by the EBM process, because for the remaining friction pairs a friction-induced increase in the Sz parameter value was observed (9.7–18.1% for 145Cr6/DC01 and 7.1–3.9% for 145r6+EBM+IO friction pair). The effect of the roller mounting type on changes in the maximum profile height is not unambiguous. Except for the friction pair 145Cr6+IO/DC01, friction involving a freely rotating CS caused a greater change in the Sz parameter compared to the as-received surface.

The parameter Sku describes the shape of the surface height distribution. The initial kurtosis value of the sheet surface in the as-received state (Sku = 5.89) indicates that the surface contained numerous deep valleys and/or many sharp peaks. Under such conditions, adhesive and abrasive wear of asperity summits dominates during frictional contact. As a result of the friction process involving all the analyzed friction pairs, a decrease in the kurtosis Sku was observed (Figure 7c). A value of Sku = 3 corresponds to a normally distributed surface profile. The most pronounced reduction in kurtosis occurred for rollers subjected to the electron beam melting (EBM) process. The skewness Ssk indicates whether peaks or valleys dominate the surface topography. The negative skewness value of the sheet in the as-received state (Ssk = −1.01) signifies the predominance of valleys in the roughness profile. At the same time, due to the limited number of peaks, the real contact area is larger and the contact pressures are higher [21]. As a result

Table 1. Comparison of CoF values for selected sample elongation values

CS material	Sample elongation ε = 6%			Sample elongation ε = 8%			Sample elongation ε = 10%			Sample elongation ε = 12%		
	Eq. 3	Eq. 5	D, %	Eq. 3	Eq. 5	D, %	Eq. 3	Eq. 5	D, %	Eq. 3	Eq. 5	D, %
145Cr6	0.31 ±0.011	0.322 ±0.008	3.72	0.302 ±0.011	0.328 ±0.005	2.43	0.317 ± 0.008	0.35 ±0.008	5.36	0.293 ±0.008	0.312 ±0.011	6.24
145Cr6 + EBM	0.28 ±0.007	0.26 ±0.008	2.09	0.306 ±0.012	0.295 ±0.009	−2.72	0.291 ± 0.011	0.279 ±0.011	−11	0.299 ±0.012	0.279 ±0.005	−7.35
145Cr6+IO	0.265± 0.011	0.255 ±0.010	−43.72	0.279 ±0.012	0.26 ±0.006	−7.50	0.266 ± 0.011	0.251 ±0.007	−5.97	0.259 ±0.010	0.241 ±0.007	−7.47
145Cr6 + EBM + IO	0.294 ±0.008	0.321 ±0.009	8.39	0.295 ±0.008	0.322 ±0.010	8.38	0.298 ± 0.006	0.327 ±0.010	8.71	0.285 0.011	0.291 ±0.010	2.06

of the friction process combined with longitudinal deformation of the specimens, the skewness value increased (Figure 7c) toward a symmetric distribution (Ssk = 0). Lower values of skewness Ssk were observed during friction involving a stationary roller. Changes in surface roughness parameters reflect not only the influence of friction mechanisms and specimen elongation, but also changes in the mechanical properties of asperity summits due to the strain-hardening phenomenon [22]. The modification of mechanical properties determines the intensity and nature of mechanisms such as flattening, ploughing, adhesive wear, and abrasive wear [23]. Figure 8 presents the surface topographies of the sheets after the friction process.

The Abbott–Firestone curve is used to evaluate the tribological properties of surfaces subjected to friction and describes the material distribution within the profile. The core roughness depth Rk was estimated based on the Abbott–Firestone curves for all profiles by imposing the minimum range of the asperity height distribution (AHD) within the interval <5%, 95%> [24]. The parameter Rk = c2 − c1 characterizes the core material portion (load-bearing area) of the surface. The parameter c1 represents the Mr1 threshold as the minimum AHD. For this threshold, the material ratio of the primary profile, Pmr(c1), equals 5%. The parameter c2 represents the Mr2 threshold as the maximum AHD. For this threshold, the material ratio of the primary profile, Pmr(c2), equals 95.0%. The parameter Rk is a measure of the surface's load-carrying capacity during friction.

The friction conditions in most tests led to an increase in the Rk parameter, ranging from 4.6% (145Cr6/DC01, stationary CS) to 24.5%

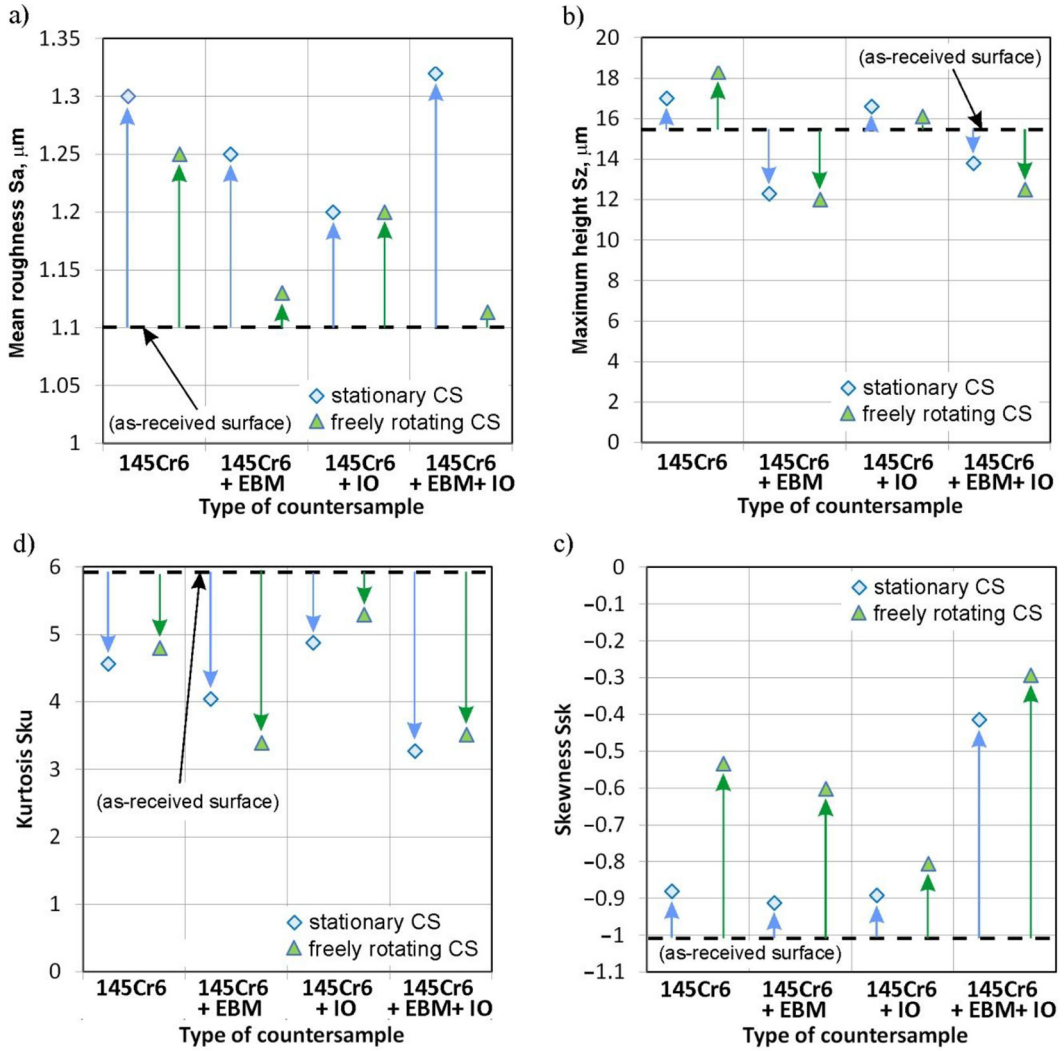

Figure 7. Influence of the type of CS on the friction-induced change of selected surface roughness parameters of samples: a) Sa, b) Sz, c) Sku and d) Ssk

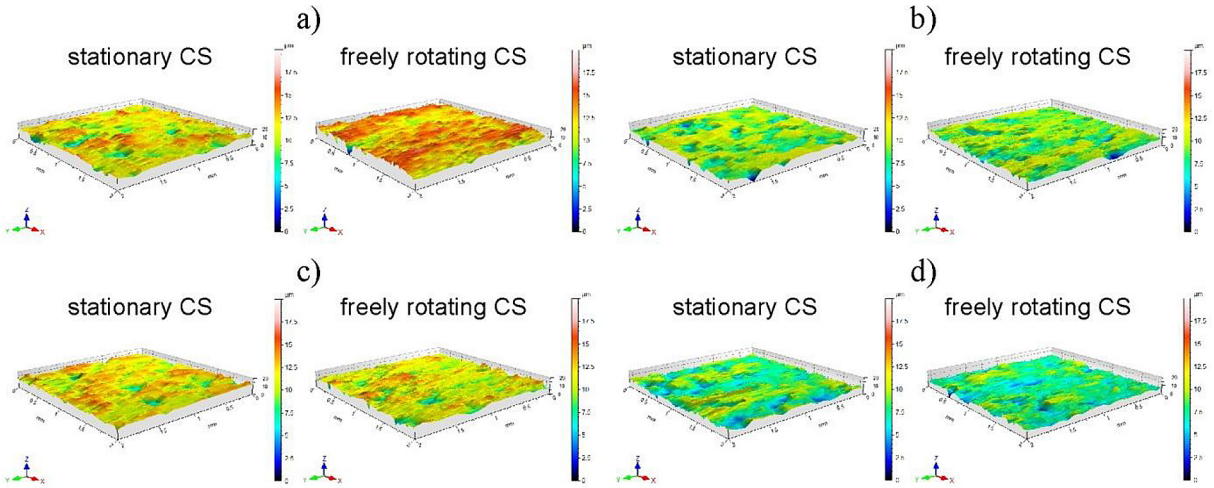

Figure 8. Surface topographies of strip samples after friction tests with the following CSs: a) 145Cr6, b) 145Cr6+EBM, c) 145Cr6+IO and d) 145Cr6+EBM+IO

Table 2. Comparison of Abbott-Firestone curve parameter values

CS material	Type of CS	c1, μm	c2, μm	Rk = c2 − c1, μm	Pmr(c1), %	Pmr(c2), %
145Cr6	Stationary	0.22	5.67	5.45	5	95
	Freely rotating	2.55	8.49	5.95	5	95
145Cr6+EBM	Stationary	0.158	7.05	6.89	5	95
	Freely rotating	0.641	6.41	5.77	5	95
145Cr6+IO	Stationary	0.376	5.05	4.67	5	95
	Freely rotating	0.879	7.72	6.84	5	95
145Cr6+EBM+IO	Stationary	2.56	8.87	6.31	5	95
	Freely rotating	0.99	7.06	6.07	5	95

(145Cr6+EBM/DC01, stationary CS). Only the friction pair 145Cr6+IO/DC01 caused a reduction in the Rk parameter by 11.3%. In addition, it can be observed that the values of the Rk parameter for friction pairs involving an EBM-processed CS were higher under friction conditions with a stationary roller. For the remaining friction pairs (145Cr6/DC01 and 145Cr6+IO/DC01), higher values of the core roughness depth Rk were observed during friction with a freely rotating roller. A certain similarity can be noted with the conclusions regarding the effect of friction on changes in the maximum height Sz of the samples (Figure 7b). Only during friction involving EBM-processed rollers did a decrease in the Sz parameter occur. In the case of surfaces in dry contact, friction is caused by mechanical interlocking of surface asperities (roughness). A higher core roughness depth Rk indicates a greater number of asperities within the main load-bearing area (Table 2) [25].

CONCLUSIONS

This paper presents the results of a non-conventional sheet-metal bending test combined with tensile deformation, which simulates friction conditions between sheet metal and the tool in stamping dies. Various approaches to modifying the tool surface layer using electron beam melting and ion implantation processes were investigated. The main conclusions are as follows:

1. For the friction pairs 145Cr6/DC01 and 145Cr6+IO/DC01, higher CoF were obtained using Equation 5. In contrast, for the remaining friction pairs involving EBM-processed CSs, Equation 3 yielded higher CoF. An increase in sheet deformation resulted in an increase in the difference D between the CoFs determined from Equations 3 and 5, from 1.78% (ε = 6%, 145Cr6/DC01) to 8.51% (ε = 8%, 145Cr6+EBM+IO/DC01). These results clearly indicate that the surface topography

resulting from the tool-processing method affects the frictional behavior associated with the Swift bending tension FB and, consequently, the CoF.
2. The friction phenomenon caused an increase in the mean surface roughness of the sheet compared to the as-received surface (Sa = 1.10 μm). The increase ranged from approximately 1.34% (145Cr6+EBM+IO/DC01, freely rotating CS) to 16.7% (145Cr6+EBM+IO/DC01, stationary CS). As a result of the friction process, the maximum profile height increased only for the friction pairs 145Cr6/DC01 and 145Cr6+IO/DC01. Except for the friction pair 145Cr6+IO/DC01, friction involving a freely rotating CS caused a greater change in the Sz parameter compared to the as-received surface.
3. As a result of the friction process involving all the analyzed friction pairs, the kurtosis Sku decreased by 10.2–42.4% relative to the as-received surface (Sku = 5.89), depending on the friction pair and the type of CS mounting. At the same time, the friction process combined with longitudinal deformation of the specimens caused an increase in the skewness Ssk. A greater change in skewness was observed for friction involving freely rotating rollers compared to the as-received surface of the strip samples.

The results of friction tests conducted using the BUT method enable a realistic assessment of the tribological conditions occurring in sheet-metal stamping processes. Analysis of changes in the surface roughness of the sheets provides insight into the friction mechanisms present in different friction pairs, as well as into the final surface quality of the stamped parts.

The results presented in the article indicate that the surface topography of the counter-sample (CS) plays a decisive role in the friction behavior of DC01 sheet metal. If a high coefficient of friction at the punch edge is required, an uncoated CS can be used. The lowest coefficients of friction were recorded for the 145Cr6+IO/DC01 friction pair. The friction process of the 145Cr6+IO pair produced the smallest changes in mean roughness (Sa), maximum height (Sz), and kurtosis (Sku) compared to the as-received material. Therefore, if surface quality is the main quality factor under dry friction conditions, ion implantation is recommended as the final method of punch surface treatment. The difference in COF values resulting from considering Swift bending under tension ranged between -7.5% and 8.39%. It should be noted that these results refer to the friction pairs analyzed in this study. For other friction pairs and topographies, these differences may vary. In friction studies using the BUT test, it is important to be aware that different formulas for calculating the COF can result in significant quantitative discrepancies in the results.

REFERENCES

1. Behrens B.A., Hübner S., Knigge J., Voges-Schwieger K., Weilandt K. Local strain-hardening in sheet metal and forging components. Mater. Technol. 2008; 79(3): 165–171. https://doi.org/10.1002/srin.200806335
2. Fejkiel R. The effect of blankholder pressure on the amount of springback in the U-draw bending process. Adv. Mech. Mater. Eng. 2024; 41: 195–204. https://doi.org/10.7862/rm.2024.17
3. Stebner S.C., Martschin J., Arian B., Dietrich S., Feistle M., Hütter S., et al. Monitoring the evolution of dimensional accuracy and product properties in property-controlled forming processes. Adv. Ind. Manuf. Eng. 2024; 8: 100133. https://doi.org/10.1016/j.aime.2023.100133
4. Barros T.H.C., Gonzaga, I.A.D., Neto, A.S., Amaral, E.C., Gonçalves, K. A.M.B., de Matos Rodrigues, P.C., Luiz V.D. Influence of multi-pass forming on the tribological performance of AISI 430 steel sheet in deep drawing process. Adv. Mech. Mater. Eng. 2025; 42: 59–69. https://doi.org/10.7862/rm.2025.5
5. Shi R., Wang B., Yan Z., Wang Z., Dong L. Effect of surface topography parameters on friction and wear of random rough surface. *Materials* 2019; *12*: 2762. https://doi.org/10.3390/ma12172762
6. Szwajka K., Trzepieciński T., Szewczyk M., Zielińska-Szwajka J., Barlak M. Investigating resulting surface topography and residual stresses in bending DC01 sheet under tension friction test. Lubricants 2025; 13: 255. https://doi.org/10.3390/lubricants13060255
7. Żaba K., Madej M., Leszczyńska-Madej B., Trzepieciński T., Sitek R. Tribological performance of direct metal laser sintered 20MnCr5 tool steel countersamples designed for sheet metal forming application. Appl. Sci. 2025; 15(15): 8711. https://doi.org/10.3390/app15158711
8. Lachmayer R., Behrens B.A., Ehlers T., Müller P., Althaus P., Oel M., Farahmand E., Gembarski P. C., Wester H., Hübner S. Process-integrated lubrication in sheet metal forming. J. Manuf. Mater. Process. 2022; 6(5): 121. https://doi.org/10.3390/jmmp6050121

9. Wang C., Hazrati J., de Rooij M.B., Veldhuis M., Aha B., Georgiou E., et al. Temperature dependent micro-mechanics-based friction model for cold stamping processes. J. Phys. Conf. Ser. 2018; 1063: 012136. https://doi.org/10.1088/1742-6596/1063/1/012136
10. Szwajka K., Trzepieciński T., Szewczyk M., Zielińska-Szwajka J., Slota J. Surface topography-based classification of coefficient of friction in strip-drawing test using Kohonen self-organising maps. Materials 2025; 18(13): 3171. https://doi.org/10.3390/ma18133171
11. Wu Y., Recklin V., Groche P. Strain induced surface change in sheet metal forming: Numerical prediction, influence on friction and tool wear. *J. Manuf. Mater. Process.* 2021; *5*: 29. https://doi.org/10.3390/jmmp5020029
12. Bounezour H., Laouar L., Bourbia M., Ouzine B. Effects of work hardening on mechanical metal properties—experimental analysis and simulation by experiments. Int. J. Adv. Manuf. Technol. 2019; 101: 2475–2485. https://doi.org/10.1007/s00170-018-3071-x
13. Wenzloff G.J., Hylton T.A., Mattock D.K. Technical note: A new test procedure for the bending under tension friction test. J. Mater. Eng. Perform. 1992; 1: 609–613. https://doi.org/10.1007/BF02649242
14. Han S.S. Influence of tool geometry on friction behavior in sheet metal forming. J. Mater. Process. Technol. 1997; 63: 129–33. https://doi.org/10.1016/S0924-0136(96)02612-X
15. Duncan J.L., Shabel B.S., Filho J.G. A tensile strip test for evaluating friction in sheet metal forming; SAE Tech. Paper 1978: 780391. https://doi.org/10.4271/780391
16. Fox R.T., Maniatty A.M., Lee D. Determination of friction coefficient for sheet materials under stretch-forming conditions. Metall. Trans. A 1989; 20: 2179–82. https://doi.org/10.1007/BF02650306
17. Andreasen J.L., Olsson D.D., Chodnikiewicz K., Bay N. Bending under tension test with direct friction measurement. Proc. Inst. Mech. Eng. Part B: J. Eng. Manuf. 2006; 220(1): 73–80. https://doi.org/10.1243/095440505X32913
18. *Gierzyńska* M. Tarcie, zużycie i smarowanie w obróbce plastycznej metali. 1st Ed. Warszawa: Wydawnictwa Naukowo-Techniczne; 1983.
19. Trzepieciński T., Szwajka K., Szewczyk M., Barlak M., Zielińska-Szwajka J. Effect of countersample coatings on the friction behaviour of DC01 steel sheets in bending-under-tension friction tests. Materials 2024; 17(15): 3631. https://doi.org/10.3390/ma17153631
20. Lemu H.G., Trzepieciński T. Numerical and experimental study of frictional behavior in bending under tension test. Stroj. Vestn. – J. Mech. Eng. 2013; 591: 41–49. https://doi.org/10.5545/sv-jme.2012.383
21. Wang W., Zhao Y., Wang Z., Hua M., Wei X. (2016). A study on variable friction model in sheet metal forming with advanced high strength steel. Tribol. Int. 2016; 93: 17–28. https://doi.org/10.1016/j.triboint.2015.09.011
22. Zwicker M.F.R., Spangenberg J., Bay N., Martins P.A.F., Nielsen C.V. The influence of strain hardening and surface flank angles on asperity flattening under subsurface deformation at low normal pressures. Tribol. Int. 2022; 167: 107416. https://doi.org/10.1016/j.triboint.2021.107416
23. Venema J., Beentjes P.C.J. The influence of coating porosity on friction and wear during hot stamping of AlSi coated ultra-high strength steel. IOP Conf. Ser. Mater. Sci. Eng. 2021; 1157: 012008. https://doi.org/10.1088/1757-899X/1157/1/012008
24. Bigerelle M., Iost A. A numerical method to calculate the Abbott parameters: A wear application. Tribol. Int. 2007; 40(9): 1319-1334. https://doi.org/10.1016/j.triboint.2006.12.007
25. Moyle N., Dong H., Wu H. Khripin C.Y., Hui C.Y., Jagota A. Increased sliding friction of a lubricated soft solid using an embedded structure. Tribol. Lett. 2022; 70: 2. https://doi.org/10.1007/s11249-021-01540-9